APERTURE COUPLING TO SHIELDED TRANSMISSION LINES: THEORY AND EXPERIMENT

D. A. Hill
M. L. Crawford
M. Kanda

U.S. DEPARTMENT OF COMMERCE
Technology Administration
National Institute of Standards
and Technology
Electromagnetic Fields Division
Electronics and Electrical Engineering Laboratory
Boulder, Colorado 80303

D. I. Wu

Department of Electrical and
Computer Engineering
University of Colorado
Boulder, Colorado 80309

NIST

APERTURE COUPLING TO SHIELDED TRANSMISSION LINES: THEORY AND EXPERIMENT

D. A. Hill
M. L. Crawford
M. Kanda

U.S. DEPARTMENT OF COMMERCE
Technology Administration
National Institute of Standards
and Technology
Electromagnetic Fields Division
Electronics and Electrical Engineering Laboratory
Boulder, Colorado 80303

D. I. Wu

Department of Electrical and
Computer Engineering
University of Colorado
Boulder, Colorado 80309

April 1992

CONTENTS

APERTURE COUPLING TO SHIELDED TRANSMISSION LINES: THEORY AND EXPERIMENT

D.A. Hill, M.L. Crawford, and M. Kanda
Electromagnetic Fields Division
National Institute of Standards and Technology
Boulder, CO 80303

D.I. Wu
Department of Electrical and Computer Engineering
University of Colorado
Boulder, CO 80309

Coupling through circular apertures in the shields of a coaxial air line and a TEM cell is studied theoretically and experimentally. Polarizability theory is used to compute the effective dipole moments that excite the transmission lines in the internal region. Measurements of shielding effectiveness of both structures were made in a reverberation chamber over wide frequency ranges. Agreement between theory and measurements is generally within ±10 dB. Recommendations for improvements in the measurements and theory are made for achieving closer agreement that would be desirable for an artifact standard for shielding effectiveness measurements.

Key words: aperture; coaxial air line; dipole moment; effective area; polarizability; reverberation chamber; shielding effectiveness; TEM cell.

1. INTRODUCTION

The shielding performance of cable shields [1] and connectors [2] is difficult to characterize and to measure. For frequencies below approximately 100 MHz, the surface transfer impedance provides a useful characterization of cable shields and can be measured using a quadraxial test fixture [3].

For radiated-field excitation at higher frequencies, an alternative approach is to regard the entire cable assembly as a receiving antenna. In this case the relevant quantity is the effective area A_e which is the ratio of the received power P_r to the incident power density P_d:

$$A_e = P_r/P_d. \tag{1}$$

Since P_r has units of W and P_d has units of W/m^2, A_e has units of m^2. If we normalize A_e to the effective area A_r of a reference antenna, we can also define shielding effectiveness (SE) as

$$SE = -10 \log_{10}(A_e/A_r), \text{ dB.} \tag{2}$$

In this report we present theoretical and experimental results for coupling through small circular apertures in the shields of a coaxial air line and a transverse electromagnetic (TEM) cell [4]. Hoeft and Hofstra [3] have made surface transfer impedance measurements on a coaxial line at frequencies below 100 MHz. In our theory and measurements we are considering higher frequencies (above 100 MHz), and we include the effects of the external geometry and the terminating impedances on A_e.

The organization of this report is as follows. In Section 2.1 we give the expressions for the current and charge on a thin circular cylinder in the absence of the aperture for plane-wave excitation. The thin cylinder can be either semi-infinite or of finite length [5]. In Section 2.2 we use polarizability theory for a small circular aperture to compute the power coupled to the air line with a matched load [6]. In Section 2.3 we compare theoretical results with measurements made in a reverberation chamber. To make this comparison we have to average the theoretical results over all incidence angles and polarizations, as shown in the Appendix. In Section 2.4 we calculate the effect of shield thickness. In Section 3 we present a comparison of theory and measurements for a TEM cell with a circular aperture in the shield. Conclusions are given in Section 4.

2. COAXIAL AIR LINE

2.1 External Current and Charge

In this section we consider plane-wave excitation of a thin cylinder of radius b. The cylinder can be semi-infinite as shown in figure 1 or of finite length as shown in figure 2. The incident field $\bar{E}^i(r)$ is polarized in the xz plane and is incident in the xz plane:

$$\bar{E}^i(r) = E^i_\theta \, (\hat{x} \cos \theta_i - \hat{z} \sin \theta_i) \, e^{i\bar{k}_i \cdot \bar{r}},$$

(3)

where $\bar{k}_i = k(\hat{x} \sin \theta_i + \hat{z} \cos \theta_i)$, $k = 2\pi/\lambda$,

and λ is the free-space wavelength. The time dependence is $\exp(-i\omega t)$.

For the semi-infinite cylinder, we follow the notation and the results of Chang et al. [5]. The induced current $I(\theta_i, z)$ can be written as

$$I(\theta_i, z) = E^i_\theta \, [V(\theta_i, z) - V(\theta_i, 0) \, R(\theta_i, z) \, U(z)], \quad z > 0,$$

(4)

where the functions V, R, and U are defined in [5]. The first term in the square brackets is the current that would exist on an infinitely long cylinder, and the second term is a good approximation to the current reflected from the end. The charge density ρ per unit length can be written

$$\rho(\theta_i, z) = \frac{1}{i\omega} \frac{\partial I(\theta_i, z)}{\partial z}.$$

(5)

The z derivative of I in (5) can be easily evaluated analytically.

We can use a similar theory to analyze a cylinder of finite length 2h as shown in figure 2. By summing the multiply reflected currents from the

3

ends, Chang et al. [5] have derived the following expression for the induced current $I(\theta_i, z)$:

$$I(\theta_i, z) = E_\theta^i \{V(\theta_i, z) + [\Delta(\pi - \theta_i, h - z)V(\theta_i, h)$$

$$+ \frac{R(\pi, h-z)}{R(\pi, 2h)}C(\pi - \theta_i)] \ U(h-z) \tag{6}$$

$$+ [\Delta(\theta_i, h+z)V(\pi - \theta_i, h) + \frac{R(\pi, h+z)}{R(\pi, 2h)}C(\theta_i)] \ U(h+z)\}, \quad |z| < h,$$

where the functions V, Δ, R, and C are defined in [5]. The charge per unit length can again be obtained by differentiation as indicated in eq (5).

2.2 Received Power

In this section we consider coupling from the external region to an internal coaxial air line through a small circular aperture. We specialize the theory of Taylor and Harrison [6] to the case of matched terminations to correspond to our experimental configuration. The geometry for a circular aperture of radius a in a semi-infinite cylinder is shown in figure 3.

For a sufficiently small radius a, the excitation of the coaxial line is that of a radial electric dipole p_{ey} and an x-directed magnetic dipole p_{mx} [6]:

$$P_{ey} = \frac{\alpha_e \ \rho(\theta_i, z_0)}{2\pi b} \quad \text{and} \quad P_{mx} = \frac{\alpha_m \ I(\theta_i, z_0)}{2\pi b},$$

$$\tag{7}$$

where $\alpha_e = 2a^3/3$ and $\alpha_m = 4a^3/3$.

The results in eq (7) can also be used for the finite-length cylinder by using the appropriate expressions for ρ and I. The dipole moments in (7)

4

produce an equivalent voltage source e_g and an equivalent current source i_g [6,7]

$$e_g = \frac{-ik\eta p_{mx}}{4\pi b} \quad \text{and} \quad i_g = \frac{ikp_{ey}}{4\pi\epsilon bZ_c},$$ (8)

where $\eta = (\mu/\epsilon)^{1/2}$, μ is the permeability of free space, ϵ is the permittivity of free space, and Z_c is the characteristic impedance of the coaxial air line.

Since the air line is terminated in its characteristic impedance at $z = 0$ and $z = s$, there are no reflections. The current in the load at $z = s$ simplifies to [6]

$$I(s) = \frac{\exp[ik(s-z_0)] \, [e_g + Z_c i_g]}{2Z_c}.$$ (9)

The power P_r received in the load at $z = s$ is

$$P_r = |I(s)|^2 Z_c, \quad \text{where} \quad |I(s)|^2 = |e_g + Z_c i_g|^2/(4Z_c^2).$$ (10)

Since the line is assumed lossless and the load is matched, P_r is independent of s.

The incident power density P_d is

$$P_d = |E_\theta^i|^2/\eta.$$ (11)

We write the effective area as $A_e(\theta_i)$ to indicate that it depends on θ_i

$$A_e(\theta_i) = [\eta|I(s)|^2]/[Z_c|E_\theta^i|^2].$$ (12)

5

As indicated in the Appendix, the effective area should be averaged over all incidence angles and polarizations to obtain the response in a reverberation chamber. Since A_e is independent of the azimuthal angle ϕ_i, the ϕ_i averaging has no effect. Since A_e is approximately zero for a ϕ-polarized incident wave, the polarization averaging introduces a factor of 1/2 which is consistent with the result of Tai [8]. Consequently the average value $\langle A_e \rangle$ is

$$\langle A_e \rangle = \frac{1}{4} \int_0^\pi A_e(\theta_i) \sin \theta_i \, d\theta_i. \tag{13}$$

The integration in eq (13) can be carried out numerically. For the semi-infinite cylinder there is a singularity at $\theta_i = \pi$ because $I(\pi, z)$ is singular [5]. However, it is an integrable singularity and causes no problem in the evaluation of eq (13). For the finite-length cylinder there is no singularity [5].

The average effective area $\langle A_r \rangle$ of the reference antenna in a reverberation chamber is $\lambda^2/(8\pi)$ as shown in eq (A15) in the Appendix. Therefore we can write SE for the apertured coaxial air line as

$$SE = -10 \log_{10}[\langle A_e \rangle/(\lambda^2/8\pi)], \tag{14}$$

where $\langle A_e \rangle$ is given by (13).

2.3 Measurements in a Reverberation Chamber

Measurements of SE for an apertured air line were performed in a reverberation chamber at NIST [9] over the frequency range from 1 to 18 GHz. The parameters for the apertured coaxial air line are: line radius $b = 3.5$ mm, aperture location $z_0 = 10.7$ cm, aperture radius $a = 1$ mm, and

characteristic impedance $Z_c = 50\ \Omega$. A second air line was also constructed with a larger aperture $a = 1.5$ mm.

Comparisons of measured SE and theoretical SE calculated from eq (14) are shown in figure 4 for both aperture radii. The theory for the semi-infinite line is used in the comparison because a semi-rigid coaxial line carries the signal from the apertured section to the chamber wall and through the wall to the receiver. The section of semi-rigid line has about the same radius as the apertured section and is long compared to the distance z_0 of the aperture from the end of the line. In using the semi-infinite model, we are neglecting any reflection of the external current that occurs at the wall boundary.

The theoretical curves are fairly smooth, and this is a result of averaging over incidence angle. The measured data show rapid frequency oscillations that are characteristic of reverberation chamber data [9] and have nothing to do with the apertured coaxial air line. The most disturbing aspect of the comparison is that the theoretical curve lies well below (about 7 dB) the measured curve for the smaller aperture ($a = 1$ mm). We would actually expect the theory to be more accurate for the smaller aperture because one of the assumptions is that $a \ll b$. From the polarizability theory in eq (7), we would expect the curves for the two aperture sizes to be separated by $(1.5)^6$ or 10.6 dB. The separation between the two measured curves is clearly greater than 10.6 dB. A possible explanation in terms of the shield thickness is given in the following section.

2.4 Corrections for Shield Thickness and Chamber Geometry

The polarizability theory given in eq (7) is valid for a circular aperture in a planar sheet of zero thickness. Clearly the shield of the air line is not planar and has some nonzero thickness t. We have no simple way of correcting for the curvature of the shield (radius b), but there is an approximate correction for the shield thickness that is based on the theory of a circular waveguide below cutoff.

For a wall (shield) thickness t and aperture radius a, McDonald [10] has calculated correction factors for the electric and magnetic polarizabilities as a function of t/a. The expressions for the modified electric and magnetic polarizabilities α'_e and α'_m are

$$\alpha'_e = \alpha_e C_e \text{ and } \alpha'_m = \alpha_m C_m, \tag{15}$$

where C_e and C_m are correction factors and α_e and α_m are given in (7). For t/a = 0, $C_e = C_m = 1$. For general values of t/a, McDonald has published curves for C_e and C_m. For t/a > 0.4, the following approximate expressions can by used:

$$C_e \approx 0.825 \ e^{-2.405 \ t/a} \text{ and } C_m \approx 0.84 \ e^{-1.841 \ t/a}. \tag{16}$$

The shield thickness is approximately 0.65 mm for both apertured air lines. Because the ratio t/a is greater for the smaller aperture, the correction is also greater for that case. The corrected theoretical curves are compared with the same measured curves in figure 5.

Another effect which we can compute approximately is the effect of reflection of the external current from the chamber wall where the semi-rigid coaxial line passes through the wall. The geometry is shown in figure 6. If we use image theory to account for the wall reflection, then the effective length of the air line is 2h as shown in figure 6. This geometry matches the finite-length line shown in figure 2, and the appropriate expression for the current I is eq (6). The rest of the analysis is the same as that for the semi-infinite model. The actual value for h in the experiment is h = 1.3 m, and the theoretical curves for the image theory are shown in figure 5.

The curves for image theory and the semi-infinite model differ by less than 3 dB at most frequencies. The agreement with the measured curve is better for the smaller aperture. This is to be expected since the theory assumes that aperture radius a is small compared to b and λ.

3. TEM CELL

3.1 Theory

A cross section of a TEM cell is shown in figure 7. A circular aperture is centered in the upper wall, and the cell is tapered down to a coaxial line at each end. Again the line is terminated in a matched load at one end, and the power is received in a matched load at the other end. The apertured TEM cell does not permit a rigorous analysis because the external geometry is too complicated to compute the current density (tangential magnetic field) and charge density (normal electric field) incident on the aperture.

An approximate analysis [4] has been performed assuming that the fields incident on the aperture are equal to the free-space incident fields. The same polarizability theory as used in eq (7) was used, and a similar theory was used for excitation of the internal TEM mode by the aperture dipole moments. No averaging over incidence angles was done, but an expression for the maximum received power was derived. The maximum occurs when the incident field is propagating along the z axis with the electric field polarized in the y direction. In the case the maximum effective area A_{max} is [4]

$$A_{max} = (Z_0/\eta) \{\frac{16\ a^3}{\lambda c\ \sinh(\pi d/2c)}\}^2 ,$$ (17)

where the dimensions c and d are shown in figure 7. The septum width w does not appear explicitly in eq (17), but the characteristic impedance Z_0 depends on w [4]. Since this theory deals only with the polarization-matched case, we normalize by $\lambda^2/(4\pi)$ to get shielding effectiveness:

$$SE = -10\ \log_{10}\{(\pi Z_0/\eta)[\frac{32\ a^3}{\lambda^2 c\ \sinh(\pi d/2c)}]^2\},\ dB.$$ (18)

3.2 Measurements in a Reverberation Chamber

Measurements of SE for two apertured TEM cells were performed in the same reverberation chamber at NIST. The parameters for the smaller TEM cell are: $a = 7.5$ mm, $c = 2.75$ cm, $d = 1.35$ cm, and $Z_0 = 50$ Ω. A comparison of theory and measurements for frequencies from 100 MHz to 4 GHz is shown in figure 8. The theory in eq (18) predicts a straight line when SE is plotted as a function of log frequency. The measured curve shows fine structure which is characteristic of most measurements made in reverberation chambers. We do not expect close agreement because the theory represents maximum coupling (minimum SE) and does not include the effects of the external geometry on the fields exciting the aperture. It is fortunate that these two effects partially cancel each other. The use of the maximum coupling lowers the SE curve, and the omission of the external geometry effects raises the SE curve. We do not include the effect of wall thickness in the theory because the ratio of wall thickness to aperture radius is small.

The parameters for the larger TEM cell are: $a = 1.55$ cm, $c = d = 6$ cm, and $Z_0 = 50$ Ω. A comparison of theoretical and measured SE for frequencies from 100 MHz to 2 GHz is shown in figure 9. The theory again predicts a straight line, and the measured curve shows fine structure typical of measurements in a reverberation chamber.

The measured curves in figures 8 and 9 show some spikes at high frequencies (above about 1 GHz); these are due to higher-order mode resonances within the TEM cell [11]. Normally TEM cells are operated at frequencies below these resonances, but TEM cells are still useful at frequencies between these narrow resonances. At low frequencies (below 200 MHz), the measured curves show greater variability with frequency and drop below the theoretical curve. These low-frequency effects could be caused by lack of a sufficient number of modes in the reverberation chamber [9].

4. CONCLUSIONS AND RECOMMENDATIONS

Shielding effectiveness has been measured for apertured coaxial air lines and TEM cells in a reverberation chamber. Polarizability theory for circular apertures has been used to calculate coupling into both types of shielded transmission lines. The theory of the coaxial air line is more rigorous because it includes the effects of the external geometry on the excitation of the circular aperture. The theory also uses averaging over incidence angle and polarization for comparison with measurements made in a reverberation chamber. The theory for the TEM cell does not include these features because the external geometry is too complicated for analysis.

Comparisons of theoretical and measured shielding effectiveness for both transmission line geometries show qualitative agreement for the frequency dependence. However, the theoretical curves are smooth, and the measured curves show rapid frequency oscillations of about ±6 dB; these are representative of the reverberation chamber. There are also some systematic differences. The theory for the coaxial line shows a slightly higher average value of shielding effectiveness than the measured data, and the theory for the TEM cell shows a greater frequency slope than the measured data. In general the theory and measurements agree within about ±10 dB, but this agreement is not achieved at all frequencies.

If an apertured shielded transmission line is to be used as an artifact standard for shielding effectiveness measurements, it would be desirable to improve the agreement between theory and measurements. The potential for improvement is greater for the coaxial air line because a more rigorous theory is available. For this geometry it is important to have an aperture radius that is small compared to the radius of the line and the wavelength. In figure 5 the agreement is better for the smaller aperture radius. It would also be desirable to have the thickness of the shield small compared to the aperture radius so that the approximate wall thickness correction [10] would be negligible in the theory. Also, the polarizability theory might be improved by using Collin's correction [12] to achieve power conservation in the coupling calculation.

The most important improvement of all would be to eliminate the section of semi-rigid coaxial cable that carries the air line signal to and through

11

the chamber wall to the receiver. The theory for the finite-length air line is available in eq (6), and the measurement variability should be reduced by eliminating the section of semi-rigid line that passes through the chamber wall. This would be particularly important in reducing variability from one facility to another. A method to accomplish this is to detect the signal within the section of air line and to run a fiber optic line [13] through the chamber wall.

Additional SE measurements on the apertured air line should be made for plane-wave illumination in an anechoic chamber. Such measurements would allow comparison of theory and measurements as a function of incidence angle and polarization in a less complex environment. The expected angular dependence is given in eq (12). Such comparisons would allow a better understanding of the coaxial air line and might point the way to improvements in the theory.

Further improvements in measurements made in reverberation chambers would be desirable both for this SE application and other applications. The theory uses a ratio of the average powers received by the reference antenna and the apertured air line to compute SE. The measurement actually uses the peak powers (as a function of mode stirrer position) received by the reference antenna and the apertured air line to compute SE. Experimental data indicate that the offset between peak and average values is on the order of 7 to 8 dB [9] independent of the test object. This offset should cancel when ratios are taken for SE measurements. However, further study of this issue would be desirable since recent experimental data show greater offset and variability in peak values [14] and no rigorous theory is available for the relationship between peak and average values measured in reverberation chambers.

5. ACKNOWLEDGMENTS

12

6. REFERENCES

[1] Vance, E.R. Coupling to Shielded Cables. New York: Wiley, 1978.

[2] Jesch, R.L. Measurement of shielding effectiveness of cables and shielding configurations by mode-stirred techniques. IEEE Trans. Electromag. Compat., EMC-30: 222-228; 1988.

[3] Hoeft, L.O.; Hofstra, J.S. Measured electromagnetic shielding performance of commonly used cables and connectors. IEEE Trans. Electromag. Compat., EMC-30: 260-275; 1988.

[4] Wilson, P.F.; Ma, M.T. A study of techniques for measuring the electromagnetic shielding effectiveness of materials. Nat. Bur. Stand. (U.S.) Tech. Note 1095; 1986.

[5] Chang, D.C.; Lee, S.W.; Rispin, L. Simple formula for current on a cylindrical receiving antenna. IEEE Trans. Ant. Propagat., AP-26: 683-690, 1978.

[6] Taylor, C.D.; Harrison, C.W. Jr. On the excitation of a coaxial line by an incident field propagating through a small aperture in the sheath. IEEE Trans. Electromag. Compat., EMC-15: 127-131; 1973.

[7] Chang, D.C.; Harrison, C.W. Jr.; Taylor, C.D. Note regarding the propagation of electromagnetic fields through slots in cylinders. IEEE Trans. Electromag. Compat., EMC-15: 152-154; 1973.

[8] Tai, C.T. On the definition of effective aperture of antennas. IEEE Trans. Ant. Propagat., AP-9: 224-225; 1961.

[9] Crawford, M.L.; Koepke, G.H. Design, evaluation, and use of a reverberation chamber for performing electromagnetic susceptibility/vulnerability measurements. Nat. Bur. Stand. (U.S.) Tech. Note 1092; 1986.

[10] McDonald, N.A. Electric and magnetic coupling through small apertures in shield walls of any thickness. IEEE Trans. Microwave Theory Tech., MTT-20: 689-695; 1972.

[11] Crawford, M.L. Generation of EM fields using TEM transmission cells. IEEE Trans. Electromag. Compat., EMC-16: 189-195; 1974.

[12] Collin, R.E. Small aperture coupling between dissimilar regions. Electromagnetics, 2: 1-24; 1982.

[13] Kanda, M.; Masterson, K.D. Optically sensed EM field probes for pulsed fields. Proc. IEEE, 80: 209-215; 1992.

[14] Kostas, J.G.; Boverie, B. Statistical model for a mode-stirred chamber. IEEE Trans. Electromag. Compat., EMC-33: 366-370; 1991.

[15] Kerns, D.M. Plane-wave, scattering-matrix theory of antennas and antenna-antenna interactions. Washington, D.C.: Nat. Bur. Stand. (U.S.) Monograph 162; 1981.

[16] Corona, P.; Latmiral, G.; Paolini, E. Performance and analysis of a reverberating enclosure with variable geometry. IEEE Trans. Electromag. Compat., EMC-22: 2-5; 1980.

APPENDIX. RANDOM FIELD EXCITATION

In this appendix we consider excitation of an arbitrary antenna by a random field with application to a mode-stirred chamber. A physical interpretation of the random field is that each member of the ensemble corresponds to a different tuner position. Thus ensemble averages correspond to averages over all tuner positions.

The geometry for an arbitrary antenna in an arbitrary field is shown in Fig. 10. We represent the incident field $\overline{E}(\overline{r})$ as an integral of plane waves over all real angles

$$\overline{E}(\overline{r}) = \int_{4\pi} \overline{F}(\Omega) \ e^{i\overline{k}\cdot\overline{r}} \ d\Omega, \tag{A1}$$

where the solid angle Ω is shorthand for the elevation and azimuth angles, α and β, and $d\Omega = \sin\alpha \ d\alpha \ d\beta$. The wavenumber $\overline{k}$ is

$$\overline{k} = -k \ (\hat{x} \ \sin\alpha \ \cos\beta + \hat{y} \ \sin\alpha \ \sin\beta + \hat{z} \ \cos\alpha). \tag{A2}$$

The spectrum $\overline{F}(\Omega)$ can be written

$$\overline{F}(\Omega) = \hat{\alpha} \ F_\alpha(\Omega) + \hat{\beta} \ F_\beta(\Omega), \tag{A3}$$

where $\hat{\alpha}$ and $\hat{\beta}$ are unit vectors that are orthogonal to each other and to $\overline{k}$.

The square of the absolute value of $\overline{E}$ can be written

$$|\overline{E}(\overline{r})|^2 = \iint_{4\pi} [\hat{\alpha}_1 F_\alpha(\Omega_1) + \hat{\beta}_1 F_\beta(\Omega_1)] \cdot [\hat{\alpha}_2 F_\alpha^*(\Omega_2) + \hat{\beta}_2 F_\beta^*(\Omega_2)]$$

$$\cdot \; e^{i(\bar{k}_1 - \bar{k}_2) \cdot \bar{r}} \; d\Omega_1 \; d\Omega_2,$$

where * indicates complex conjugate. We now introduce the following random-field assumptions

$$<F_\alpha(\Omega_1) F_\alpha^*(\Omega_2)> = <F_\beta(\Omega_1) F_\beta^*(\Omega_2)> = \frac{|E_0|^2}{8\pi} \; \delta(\Omega_1 - \Omega_2),$$

<div align="right">(A5)</div>

$$<F_\alpha(\Omega_1) F_\beta^*(\Omega_2)> = <F_\beta(\Omega_1) F_\alpha^*(\Omega_2)> = 0,$$

where $< \; >$ indicates ensemble average, E_0 is a constant, and δ is the Dirac

delta function. We can evaluate $<|\bar{E}(\bar{r})|^2>$ by substituting (A5) into (A4)
and using the property of the delta function to evaluate one integration.
The second integration is easily evaluated as follows

$$<|\bar{E}(\bar{r})|^2> = \int_{4\pi} \frac{|E_0|^2}{4\pi} \; d\Omega_1 = |E_0|^2. \tag{A6}$$

Thus the mean-square value of the electric field is $|E_0|^2$ and is independent
of position. The average power density $<P_d>$ is also independent of position

$$<P_d> = |E_0|^2/\eta. \tag{A7}$$

The received signal b_0 of an arbitrary receiving antenna can be
written in a form which is analogous to Kerns' plane-wave, scattering-matrix
notation [15]

$$b_0 = \int_{4\pi} \bar{S}(\Omega) \cdot \bar{F}(\Omega) \; d\Omega, \tag{A8}$$

where the spectrum $\overline{F}(\Omega)$ is given by (A3) and the receiving function $\overline{S}(\Omega)$ can be written in component form

$$\overline{S}(\Omega) = \hat{\alpha}\, S_{\alpha}(\Omega) + \hat{\beta}\, S_{\beta}(\Omega).$$ (A9)

The received power is proportional to $|b_0|^2$ which can be written

$$|b_0|^2 = \iint_{4\pi} [S_{\alpha}(\Omega_1)F_{\alpha}(\Omega_1) + S_{\beta}(\Omega_1)F_{\beta}(\Omega_1)]\ [S_{\alpha}^*(\Omega_2)F_{\alpha}^*(\Omega_2) +$$

(A10)

$$+\ S_{\beta}^*(\Omega_2)F_{\beta}^*(\Omega_2)]\ d\Omega_1\ d\Omega_2.$$

If we substitute (A5) into (A10) and carry out the Ω_2 integration, we obtain the following average value

$$<|b_0|^2> = \frac{1}{2}\,|E_0|^2\,\frac{1}{4\pi}\int_{4\pi} [|S_{\alpha}(\Omega_1)|^2 + |S_{\beta}(\Omega_1)|^2]\ d\Omega_1.$$ (A11)

On the right side of (A11), 1/2 results from polarization mismatch [8], $|E_0|^2$ is the mean square value of the incident electric field, and the Ω_1 integral is the average value of $|\overline{S}|^2$ over all incidence angles. Thus the directional characteristics of $\overline{S}(\Omega_1)$ are averaged out.

The result in (A11) can be used to obtain two results of practical interest. For the case of aperture coupling to a coaxial line considered in this paper, the S_{β} component is zero, and the S_{α} component is independent of azimuthal angle β. Thus the β integration yields a factor of 2π, and only the integration over elevation angle remains. In the notation of Section 2.2, the average value of effective area is then given by (13).

For a more general receiving antenna, we can use the result in (A11)' to determine the average value of received power $<P_r>$. For a lossless,

16

impedance-matched antenna with radiation resistance R_r, we can use (A11) to write

$$<P_r> = \frac{<|b_0|^2>}{R_r} = \frac{1}{2} <P_d> \frac{1}{4\pi} \int_{4\pi} \frac{\eta}{R_r} [|S_\alpha(\Omega_1)|^2 + |S_\beta(\Omega_1)|^2] \, d\Omega_1, \tag{A12}$$

where we have used (A7) to introduce the average power density $<P_d>$. We can relate the integrand of (A12) to the effective area of an isotropic antenna $\lambda^2/4\pi$ and the gain $G(\Omega_1)$ by

$$\frac{\eta}{R_r} [|S_\alpha(\Omega_1)|^2 + |S_\beta(\Omega_1)|^2] = \frac{\lambda^2}{4\pi} G(\Omega_1). \tag{A13}$$

If we substitute (A13) into (A12), we obtain

$$<P_r> = \frac{1}{2} <P_d> \frac{\lambda^2}{4\pi} \frac{1}{4\pi} \int_{4\pi} G(\Omega_1) \, d\Omega_1. \tag{A14}$$

The Ω_1 integration in (A14) is easily evaluated because the average value of G is one. Thus the desired result for $<P_r>$ is

$$<P_r> = \frac{1}{2} <P_d> \frac{\lambda^2}{4\pi}. \tag{A15}$$

The physical interpretation of this remarkably simple result is that the average received power is equal to average power density times the effective area $\lambda^2/4\pi$ of an isotropic antenna times a factor of 1/2 to account for polarization mismatch [8]. This result is independent of the gain and polarization characteristics of the receiving antenna and is consistent with the reverberation chamber analysis [16] of Corona et al. The result in (A15) does not apply to the apertured coaxial air line because the line has loss and is not impedance matched.
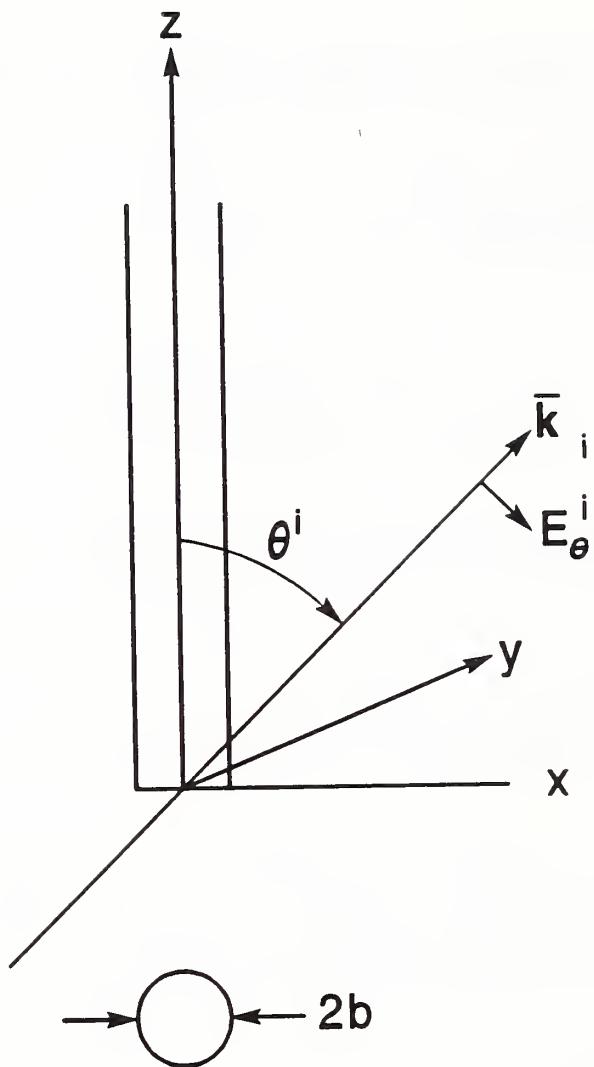
Figure 1. Plane wave incident on a semi-infinite cylinder.
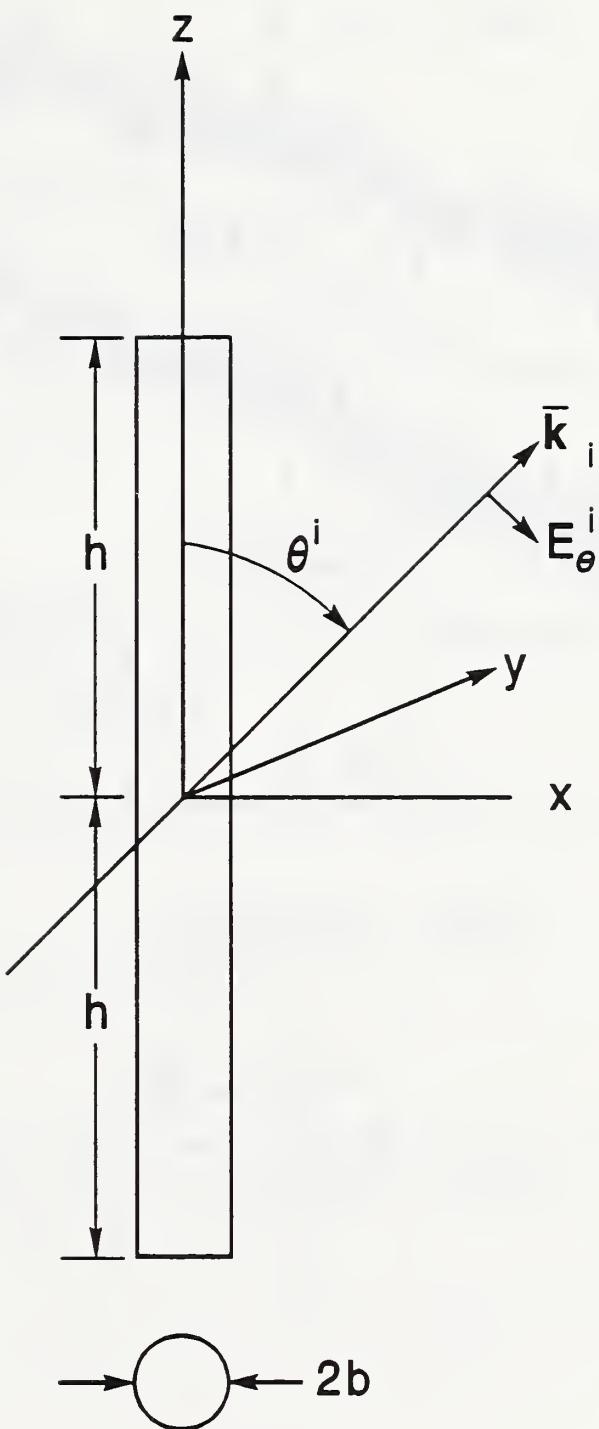
Figure 2. Plane wave incident on a cylinder of length 2h.
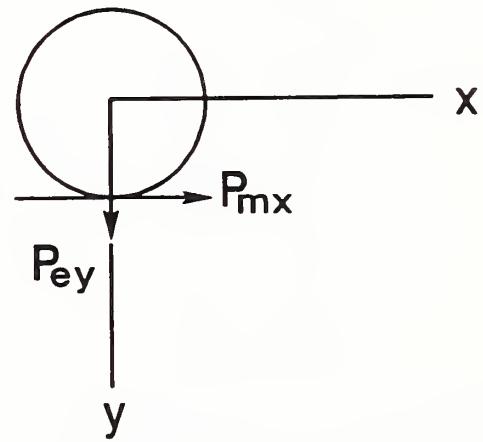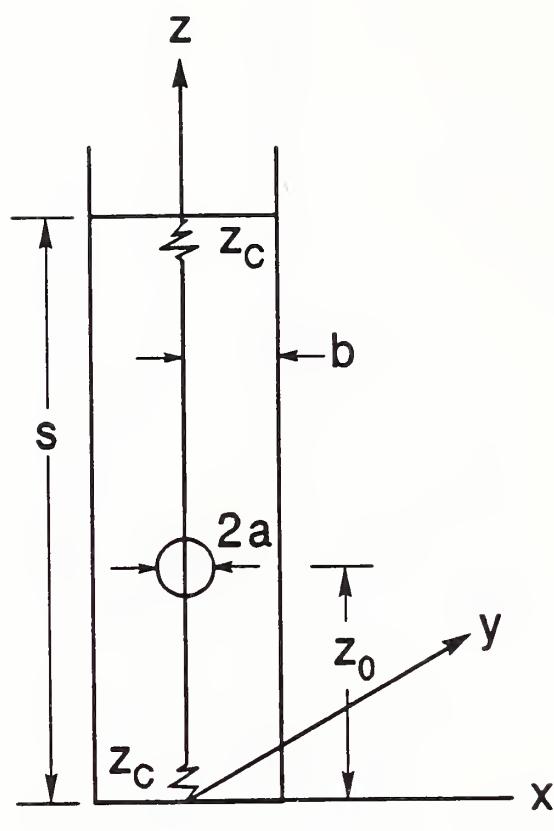
Figure 3. Electric and magnetic dipole moments induced in a circular aperture. The internal air line is terminated in its characteristic impedance.
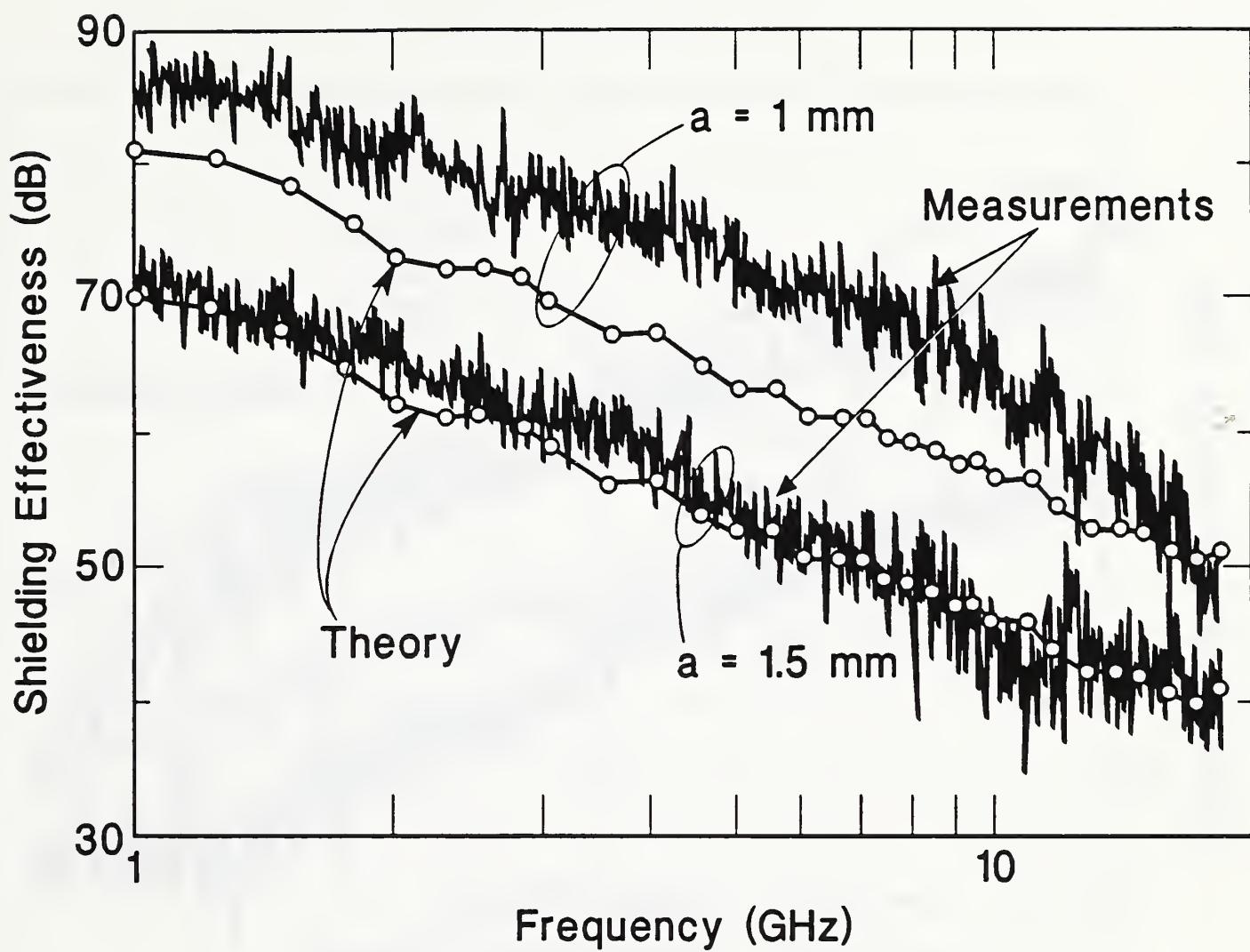
Figure 4. Theoretical and measured shielding effectiveness for a coaxial air line with a circular aperture. Parameters: $b = 3.5$ mm, $z_0 = 10.7$ cm, $Z_c = 50$ Ω.
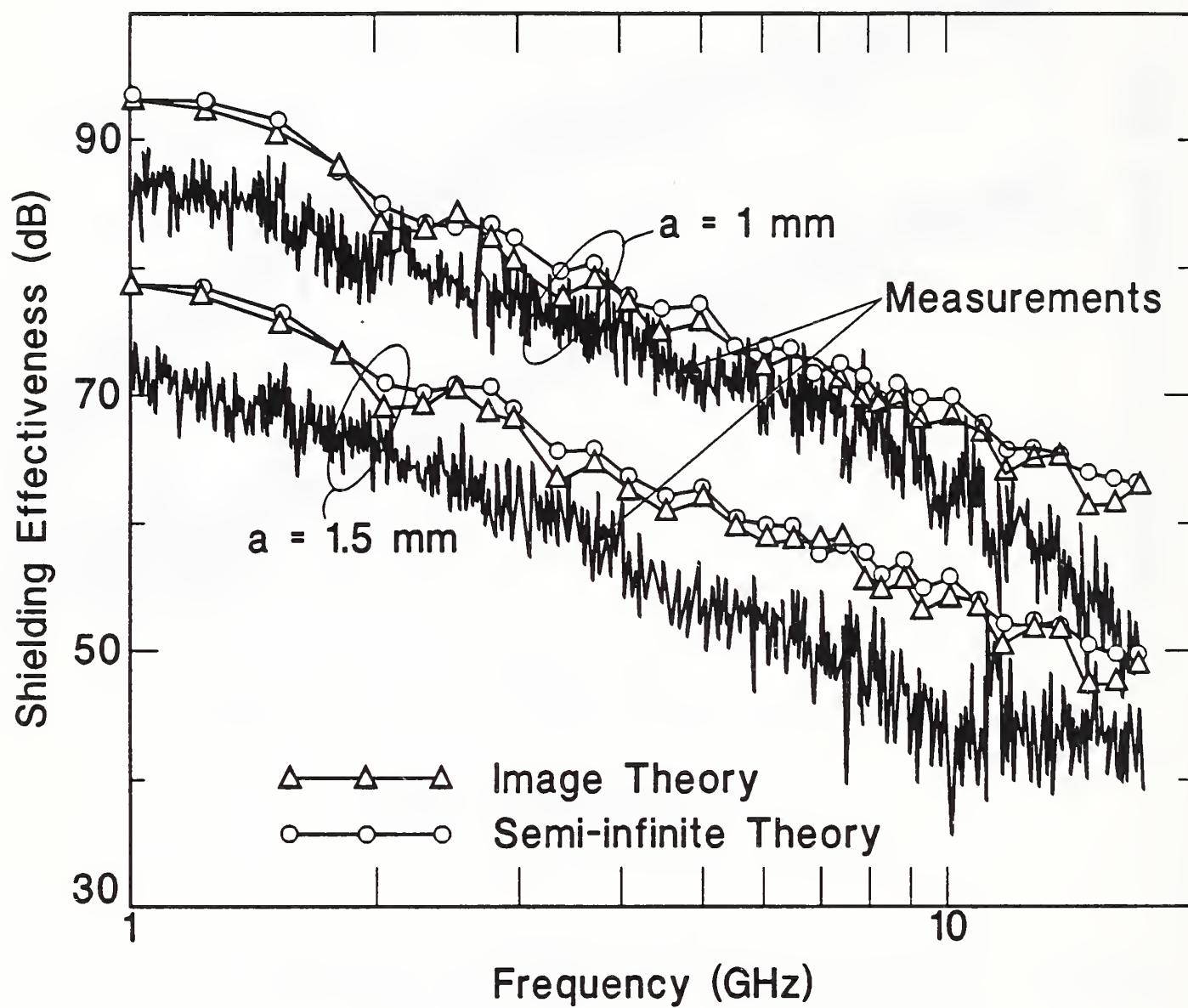
Figure 5. Semi-infinite theory, image theory, and measurements for shielding effectiveness of a coaxial air line. Both theories are modified to include wall thickness.
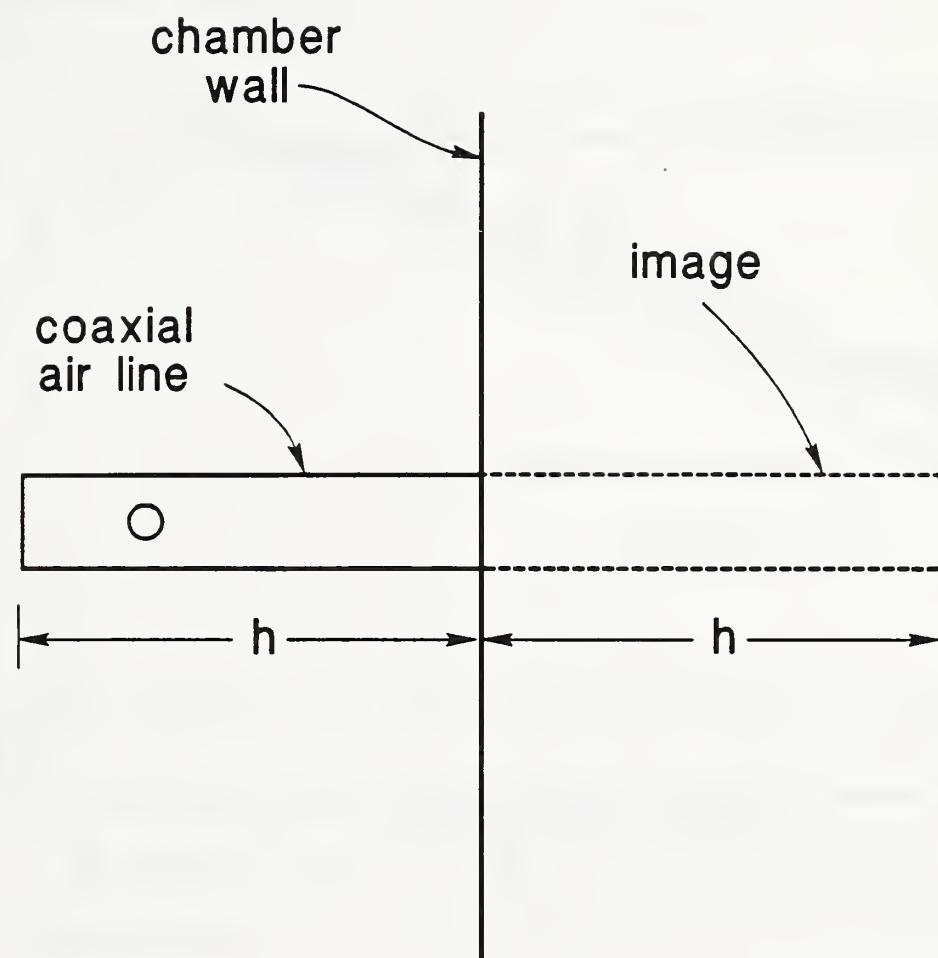
Figure 6. Geometry for an apertured coaxial air line passing through the wall in a reverberation chamber. The image accounts for reflection of external currents at the wall boundary.
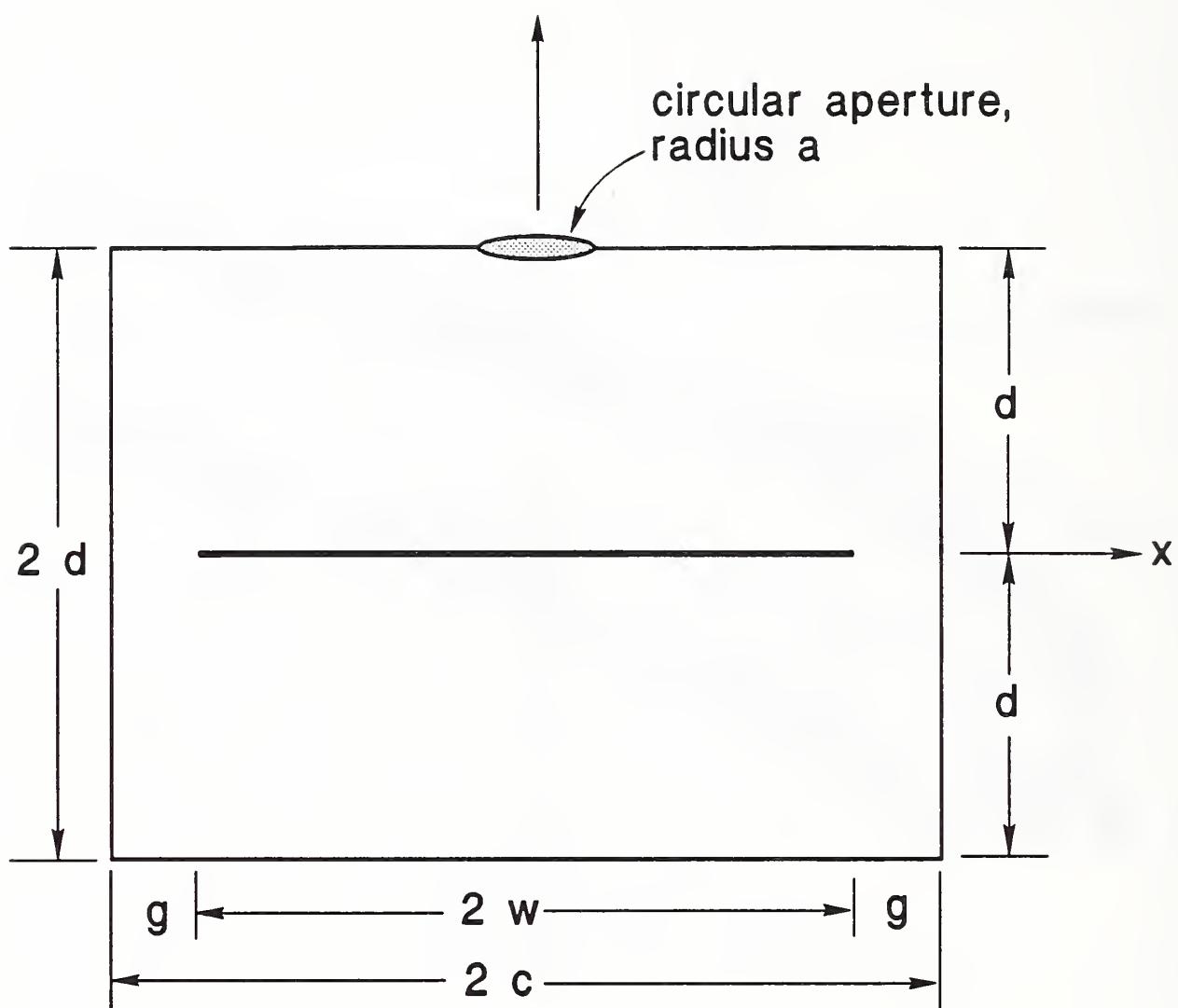
Figure 7. Geometry for an apertured TEM cell.
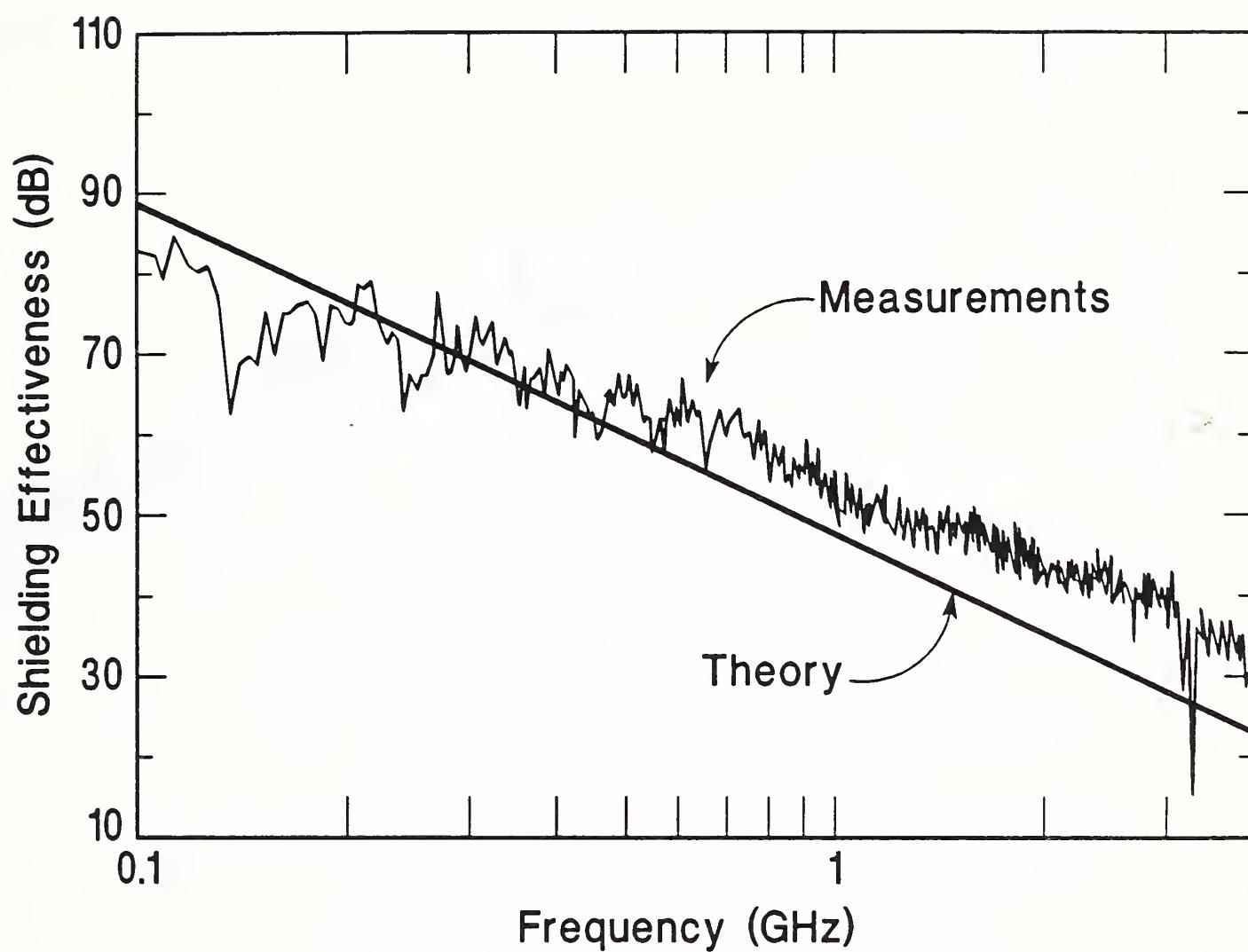
Figure 8. Theoretical and measured shielding effectiveness for a TEM cell with a circular aperture. Parameters: a = 7.5 mm, c = 2.75 cm, d = 1.35 cm, Z_0 = 50 Ω.
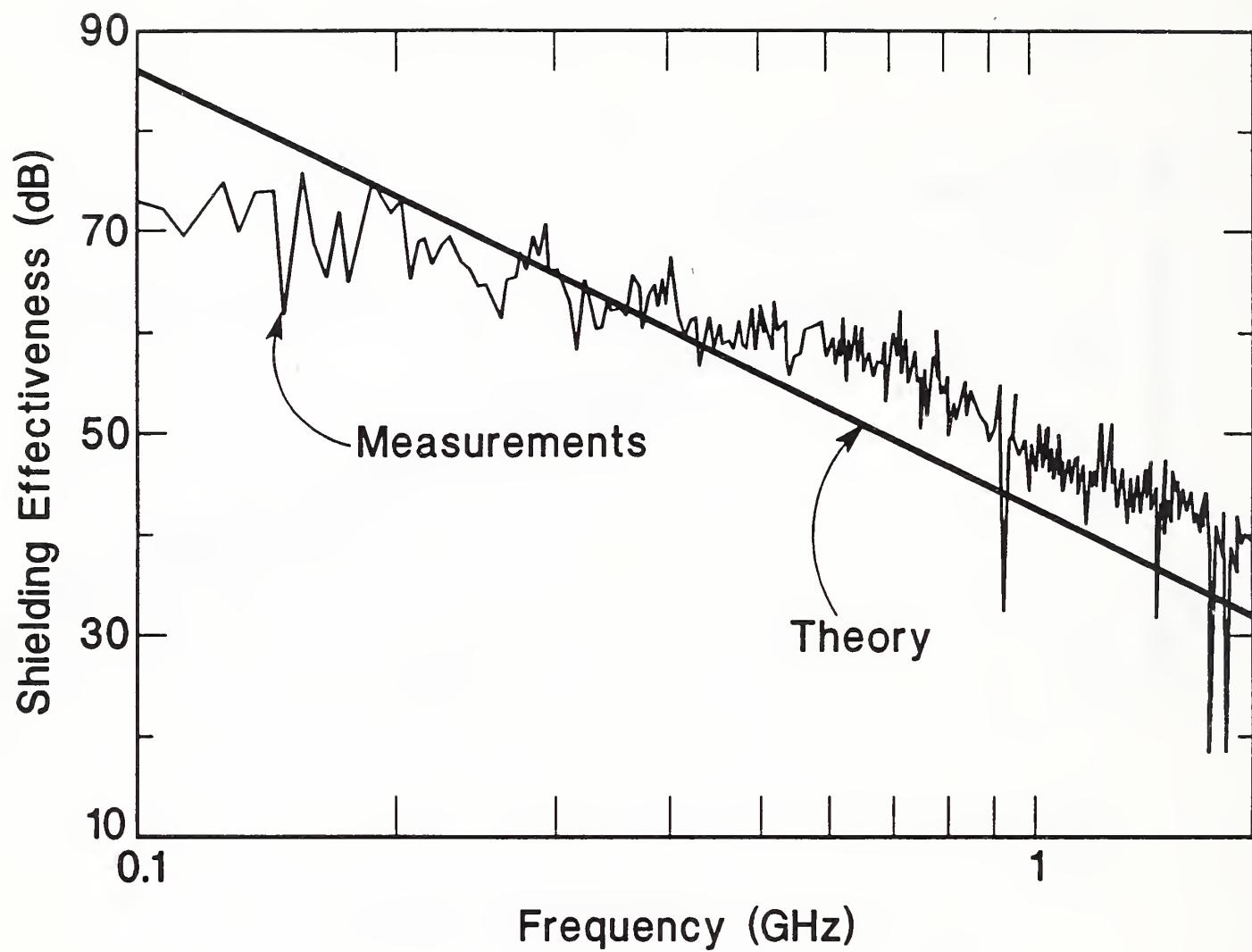
Figure 9. Theoretical and measured shielding effectiveness for a TEM cell
with a circular aperture. Parameters: a = 1.55 cm, c = d = 6 cm,
Z_0 = 50 Ω.
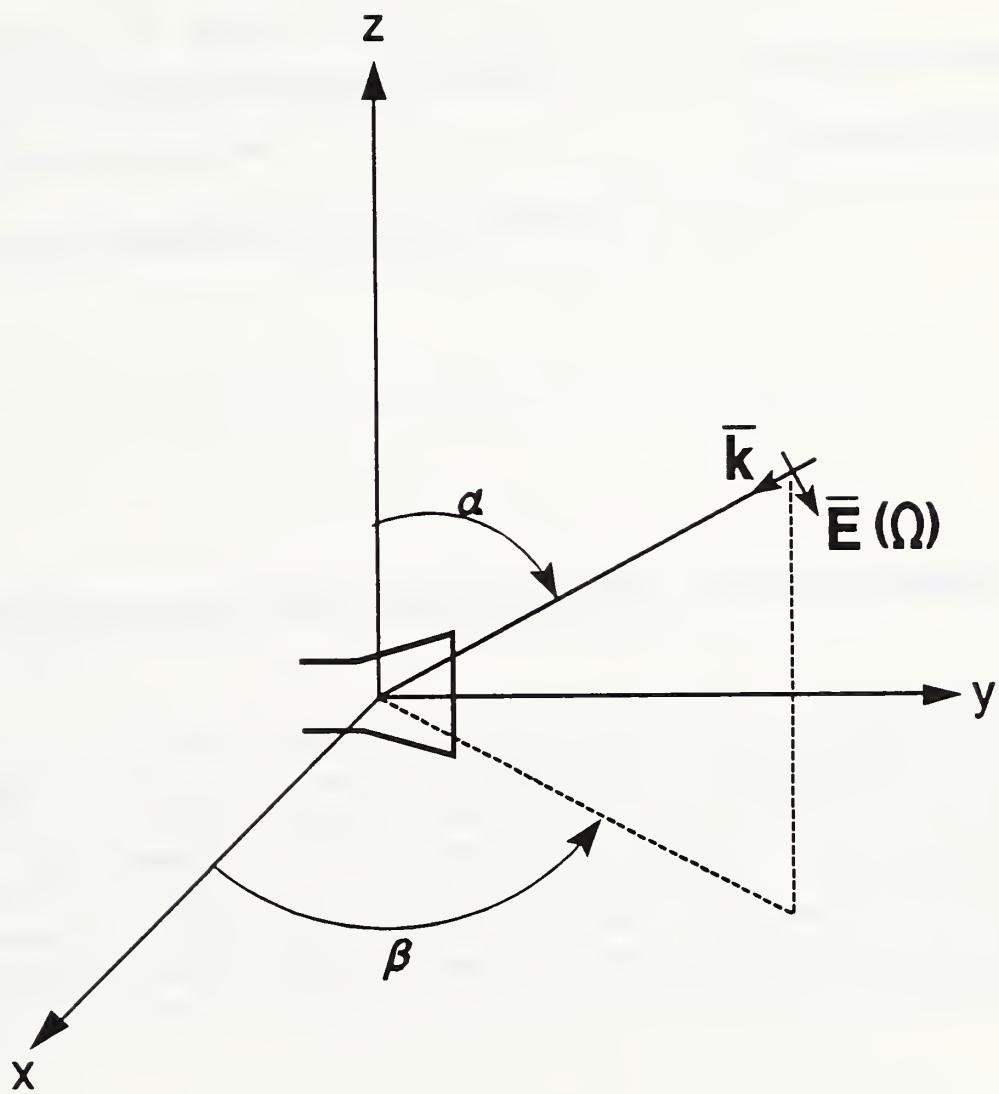
Figure 10. Plane-wave component of the electric field incident on an arbitrary receiving antenna.

4. TITLE AND SUBTITLE

Aperture Coupling to Shielded Transmission Lines: Theory and Experiment

5. AUTHOR(S)

D.A. Hill, M.L. Crawford, M. Kanda, and D.I. Wu

9. SPONSORING ORGANIZATION NAME AND COMPLETE ADDRESS (STREET, CITY, STATE, ZIP)

10. SUPPLEMENTARY NOTES

11. ABSTRACT (A 200-WORD OR LESS FACTUAL SUMMARY OF MOST SIGNIFICANT INFORMATION. IF DOCUMENT INCLUDES A SIGNIFICANT BIBLIOGRAPHY OR LITERATURE SURVEY, MENTION IT HERE.)

Coupling through circular apertures in the shields of a coaxial air line and a TEM cell is studied theoretically and experimentally. Polarizability theory is used to compute the effective dipole moments that excite the transmission lines in the internal region. Measurements of shielding effectiveness of both structures were made in a reverberation chamber over wide frequency ranges. Agreement between theory and measurements is generally within $\pm$ 10 dB. Recommendations for improvements in the measurements and theory are made for achieving closer agreement that would be desirable for an artifact standard for shielding effectiveness measurements.

12. KEY WORDS (6 TO 12 ENTRIES; ALPHABETICAL ORDER; CAPITALIZE ONLY PROPER NAMES; AND SEPARATE KEY WORDS BY SEMICOLONS)

aperture; coaxial air line; dipole moment; effective area; polarizability; reverberation chamber; shielding effectiveness; TEM cell

13. AVAILABILITY	14. **NUMBER OF PRINTED PAGES**
[X] UNLIMITED	30
[ ] FOR OFFICIAL DISTRIBUTION. DO NOT RELEASE TO NATIONAL TECHNICAL INFORMATION SERVICE (NTIS).	
[ ] ORDER FROM SUPERINTENDENT OF DOCUMENTS, U.S. GOVERNMENT PRINTING OFFICE, WASHINGTON, DC 20402.	15. **PRICE**
[X] ORDER FROM NATIONAL TECHNICAL INFORMATION SERVICE (NTIS), SPRINGFIELD, VA 22161.	A02

ELECTRONIC FORM